

25 **Abstract**

26 The Multi-Angle Implementation of Atmospheric Correction (MAIAC) algorithm is under evaluation
27 for use in conjunction with the Geostationary Coastal and Air Pollution Events (GEO-CAPE) mission.
28 Column aerosol optical thickness (AOT) data from MAIAC are compared against corresponding data
29 from the Visible Infrared Imaging Radiometer Suite (VIIRS) instrument over North America during
30 2013. Product coverage and retrieval strategy, along with regional variations in AOT through
31 comparison of both matched and un-matched seasonally gridded data are reviewed. MAIAC shows
32 extended coverage over parts of the continent when compared to VIIRS, owing to its pixel selection
33 process and ability to retrieve aerosol information over brighter surfaces. To estimate data accuracy,
34 both products are compared with AERONET Level 2 measurements to determine the amount of error
35 present and discover if there is any dependency on viewing geometry and/or surface characteristics.
36 Results suggest that MAIAC performs well over this region with a relatively small bias of -0.01;
37 however there is a tendency for greater negative biases over bright surfaces and at larger scattering
38 angles. Additional analysis over an expanded area and longer time period are likely needed to determine
39 a comprehensive assessment of the products capability over the Western Hemisphere.

40 **Index Terms:**

41 Aerosols and particles

42 Remote sensing

43 **Keywords:**

44 MAIAC, Suomi-NPP VIIRS, Aerosol Optical Thickness, Intercomparison, Evaluation

45

46

47 **1. Introduction**

48 Aerosols are a key component of the Earth's climate and environmental system due to their impact on
49 the radiative budget of the planet and influence on air quality events [*Ramanathan et al.*, 2001].
50 Information on the amount and composition of the aerosol particles suspended in the atmosphere is
51 required to understand their role as both direct contaminants and precursors to air pollution [*Wang and*
52 *Christopher*, 2003; *Al-Saadi et al.*, 2005]. The GEO-CAPE mission was recommended by the National
53 Research Council's 2007 Decadal Survey in order to provide multiple observations per day in support of
54 the atmospheric composition and coastal biophysics disciplines [*NRC*, 2007]. Many current sensors
55 dedicated toward atmospheric composition sit in Low Earth Orbit (LEO) and have only one daytime and
56 one nighttime overpass for a given location when more frequent measurements are needed to fully
57 monitor the emission of pollutants and their transport. A geostationary platform provides both the
58 temporal and spatial resolution needed to understand the conditions and processes leading to poor air
59 quality events and the necessary response [*Lahotz et al.*, 2012].

60 Originally planned as a large satellite carrying multiple instruments, GEO-CAPE has shifted toward a
61 phased implementation making use of available space on commercial geostationary satellites. This
62 utilization of hosted payloads should help to reduce risk and costs, and has been supported by both
63 science working groups [*Fishman et al.*, 2012]. The atmospheric science working group is tasked with
64 developing a strategy which allows for the observation of aerosols and trace gases for use in air quality
65 studies. The MAIAC algorithm is the current candidate to provide information on aerosols from this
66 geostationary satellite.

67 The MAIAC algorithm provides simultaneous retrievals of surface bidirectional reflectance distribution
68 function (BRDF), bidirectional reflectance factor (BRF) commonly called surface reflectance, and AOT
69 at 466 nm over clear sky and snow-free scenes using a time series of MODerate Imaging

70 Spectroradiometer (MODIS) observations. This BRDF characterization over time for varying
71 geometries is used, along with the spectral regression coefficient (SRC), to help the MAIAC algorithm
72 retrieve AOT over bright surfaces with improved accuracy [Lyapustin *et al.*, 2011].

73 Here this new generic algorithm is assessed through a comparison with the operational VIIRS aerosol
74 algorithm which uses an atmospheric correction approach. VIIRS was chosen for this comparison due to
75 the improvements over its predecessors in terms of resolution, pixel aggregation, and swath width. For
76 instance, MODIS has a long history of providing aerosol retrievals with high accuracy, but it currently
77 only produces AOT at a maximum resolution of 3 km, and has greater distortion at the swath edge when
78 compared to VIIRS. The Multi-angle Imaging Spectroradiometer (MISR) uses nine fixed-angle cameras
79 to view each location at a variety of viewing angle which allows it to also retrieve AOT over brighter
80 surfaces; however its limited swath width (400 km) and coarse resolution (17.6 km) are prohibitive to its
81 inclusion in this analysis. Ultimately, the sensor characteristics and availability of .75 km AOT retrievals
82 make it ideal for a comparison with MAIAC. In this study, a years' worth of AOT from both MAIAC
83 and VIIRS over the North American continent is analyzed to look at differences in cloud screening, bias
84 dependence and overall accuracy.

85 **2. Data**

86 **2.1 MAIAC AOT**

87 The MAIAC algorithm retrieves surface reflectance and AOT using MODIS L1B reflectances which
88 have been gridded at a 1 km resolution. It utilizes a 4-16 day time series of clear MODIS scenes to
89 retrieve BRDF and Spectral Regression Coefficients (SRC), which relates surface reflectance at
90 $0.466\mu\text{m}$ and $2.13\mu\text{m}$ (MODIS bands 3 and 7) [Lyapustin *et al.*, 2012]. Unlike MISR, which collects
91 nearly-simultaneous observations of each pixel from various angles, the MAIAC algorithm uses
92 consecutive overpasses from a single-look instrument like MODIS to acquire multi-angle sets of

93 observations for each location. The use of a time-series of gridded MODIS observations also has the
94 advantage of being able to simulate geostationary satellite observations, albeit with a significantly larger
95 time difference between images. MAIAC relies on the assumption that surface reflectance changes
96 rapidly in space but slowly in time, and therefore can be assumed constant over limited time scales. By
97 contrast, the extent of clouds and aerosols can change greatly between MODIS overpasses.

98 The following is a brief overview of the MAIAC aerosol algorithm, a more detailed description of the
99 MAIAC theoretical background and processing steps can be found in *Lyapustin et al.*, (2011). Once the
100 MODIS reflectance is gridded and split into both 600 x 600 km tiles and 25 x 25 km blocks, they are
101 placed in a queue of 4-16 days. Water vapor is first derived from MODIS near-IR bands [*Lyapustin et al.*,
102 2014] using a modification of the algorithm described in *Gao and Kauffman* (2003). An internal cloud
103 mask uses spectral reflectance and brightness temperature tests similar to the operational MODIS cloud
104 mask algorithm [*Frey et al.*, 2008], along with the reference clear-sky image developed using a covariance
105 based algorithm. Clouds can be detected since the spatial pattern of the surface often doesn't change
106 noticeably from day to day, while cloud residency is relatively short. Scenes are compared at both the
107 block and pixel level against a clear-sky reference image built using the data queue [*Lyapustin et al.*,
108 2008]. The BRDF is then retrieved at MODIS band 7 (2.1 μm) for clear pixels, followed by retrieval of
109 SRC in MODIS band 3 (0.466 μm). This retrieval of SRC gives an assessment of surface BRDF (0.466 μm)
110 at pixel level, which allows MAIAC to retrieve AOT at high 1km resolution.

111 The MAIAC algorithm provides AOT at 466 nm, however in order to compare directly with VIIRS, it
112 must be converted to AOT at 550 nm. To do this, a set of ratios representing the spectral slope of a given
113 AOT are used. These ratios, which are taken directly from the aerosol background model, are part of the
114 MAIAC look-up tables [*Lyapustin et al.*, 2011]. MODIS-based MAIAC aerosol products were produced
115 over North America for the entire MODIS record up until July 2014. MAIAC is currently at version 1,
116 and data used for this analysis was obtained from NASA on November 17, 2014.

117 2.2 VIIRS AOT

118 The Visible and Infrared Imaging Radiometer Suite (VIIRS) is a scanning radiometer carried on board
119 the Suomi-NPP (National Polar-orbiting Partnership) satellite; a joint venture between NOAA and
120 NASA meant to help transition to the Joint Polar Satellite System (JPSS), the next generation in U.S.
121 polar-orbiting satellites. The operational VIIRS AOT product is produced by the Interface Data
122 Processing System (IDPS), which takes raw instrument data from S-NPP and processes them into the
123 Sensor Data Records (SDRs) that are used as inputs for the Environmental Data Records (EDRs),
124 including AOT. The aerosol algorithm uses the dark-target approach to retrieve AOT. This method is
125 built upon the legacy of retrieving aerosol properties from previous earth sensing satellite missions
126 [Holben *et al.*, 1992; Kaufman *et al.*, 1997]. The algorithm is comprised of two distinct parts which are
127 applied based on the surface type. Over ocean, the VIIRS algorithm is nearly identical to the MODIS
128 ocean algorithm [Tanre *et al.*, 1997], which uses a combination of fine and coarse mode aerosol models
129 in attempt to replicate the top-of-atmosphere (TOA) reflectance. Over land, the VIIRS aerosol
130 algorithm is based on the MODIS Atmospheric Correction algorithm for determining surface reflectance
131 [Vermote and Kotchenova, 2008]. Aerosol information is retrieved by comparing the derived spectral
132 surface reflectance ratios to prescribed ratios of those reflectances, and chooses the aerosol model and
133 AOT that minimizes the residual. The VIIRS aerosol algorithm operates under the assumption of a
134 Lambertian surface when retrieving the surface reflectance. An overview of the VIIRS sensor and an in-
135 depth explanation of the scientific background and flow of the VIIRS aerosol algorithm are presented in
136 Jackson *et al.*, (2013).

137 The aerosol retrieval for both ocean and land is performed at the pixel resolution (750 m). This pixel
138 level product is known as the Intermediate Product (IP) as it is used to create the aggregated AOT EDR,
139 along with acting as an input for other VIIRS products. The VIIRS algorithm aggregates 8x8 arrays of
140 IP AOT pixels into a single EDR pixel with a resolution of 6 km at nadir. At the IP level, the VIIRS

141 Cloud Mask (VCM) and a series of internal checks are applied to the aerosol product, resulting in each
142 pixel being given one of four quality designations. AOT is reported only for pixels in the two best
143 quality levels (good and degraded) and therefore these are the only pixels included in the aggregation
144 process, which also incorporates additional filtering and internal checks, producing a higher quality
145 product.

146 A full year of VIIRS IP AOT spanning the time from February 1, 2013 to February 1, 2014 was used to
147 compare against the MAIAC product. The selection of this time period was predicated by data
148 availability and maturity. The VIIRS Aerosol algorithm has undergone multiple upgrades since launch
149 to improve the accuracy and precision of its retrievals. One significant upgrade was a change to the
150 spectral reflectance ratios used in the land inversion which took place in January 2013 [*Hongqing et al.,*
151 *2013*]. This greatly reduced the bias in the aerosol products over land and allowed the product to reach
152 ‘validated’ status. Because data prior to this change becoming operational are still considered
153 ‘provisional’, they were not included in this analysis. Officially, the version of the product used in this
154 study was given a maturity level of Validated Stage II in August 2014, meaning that it has been shown
155 to meet the performance thresholds [*NOAA-NESDIS, 2014*] using a moderate set of test data. There are
156 no such standards for the IP product; however it also meets the EDR requirements, making it suitable for
157 quantitative analysis.

158 Other significant changes have occurred to the AOT product after the time period used in this study
159 which had impacts on retrieval accuracy and to a lesser extent, spatial coverage. These include an
160 improvement in snow screening, spatial homogeneity tests, and the removal of the ephemeral water test
161 which often incorrectly screened out portions of heavy smoke plumes. Unfortunately due to the MAIAC
162 data record ending in mid-2014, data containing these fixes were not included in this analysis.

163 **2.3 AERONET**

164 AERONET is a global network of ground-based, automatic sky-scanning spectral radiometers used to
165 measure aerosol optical properties [Holben *et al.*, 1998]. Developed and maintained by NASA, these
166 weather resistant sun photometers are a vital source of information for aerosol research and the
167 validation of satellite derived aerosol properties. The direct-sun measurements are used to compute the
168 column AOT at a variety of wavelengths from 340 – 1020 nm, spanning a majority of the visible and
169 Near-IR spectrum. Angstrom Exponent (AE) is also retrieved using wavelength pairs in the
170 aforementioned range, along with the column water vapor. Level 2.0 AOT from AERONET sites in
171 North America are used to compare against both the MAIAC and VIIRS AOT to determine accuracy
172 and uncover any bias dependencies. Level 2 data has the highest quality assurance of all AEROENT
173 data and is cloud-cleared and fully calibrated [Smirnov *et al.*, 2000]. The “ground truth” AOT at the
174 VIIRS and MAIAC wavelengths are computed using the AERONET AOT at 500 and 440 nm
175 respectively, using the AE retrieved in the 440-675 nm range.

176 **2.4 CALIPSO**

177 The Cloud-Aerosol Lidar with Orthogonal Polarization (CALIOP) is an active lidar instrument aboard
178 the CALIPSO satellite. It provides vertically resolved information on clouds and aerosols using profiles
179 of attenuated backscatter at 532 and 1064 nm at an along track resolution of 333 meters and a vertical
180 resolution of 30 meters [Winker *et al.*, 2009]. CALIOP is able to detect the number and extent of
181 features such as aerosol or cloud layers using the backscatter profiles [Vaughan *et al.*, 2004]. The level 2
182 products are produced at the nominal resolution of 333 m as well as 1 and 5 km by aggregating
183 consecutive observations. For this study, the 1 km cloud layer products are used to verify the accuracy
184 of the MAIAC and VIIRS cloud masks and determine if any issues related to cloud screening are
185 influencing the analysis. A binary cloud mask is constructed from the ‘Number of Layers Found’
186 dataset, which simply gives the number of cloud layers found within that 1 km profile.

187 **3. Results and Discussion**

188 **3.1 Daily gridding of VIIRS and MAIAC**

189 Before assessing the MAIAC algorithm and how it compares to VIIRS, the datasets were gridded to
190 directly compare their spatial extent and the quality of AOT retrievals. A grid was constructed with a
191 0.25° resolution in order to capture as much of the AOT spatial variability while limiting computational
192 cost. The shaded domain outlined in Figure 1 shows the extent of the grid whose domain is limited by
193 the MAIAC coverage over North America, which is largely confined to the Continental U.S. and
194 Mexico. The result is a grid with dimensions of 256 x 116, or a total of 29,696 grid boxes.

195 In order to compare the best retrievals from both algorithms, a set of quality checks were applied during
196 the gridding process. To start, data from both algorithms are restricted to the highest quality retrievals
197 over land. To avoid any possible cloud leakage, the candidate pixel was required to be confidently clear
198 and not be adjacent to a cloudy pixel in order to be used for gridding. Both MAIAC and VIIRS AOT
199 have an associated geolocation file which gives the center coordinates of each pixel. The gridding
200 process averages any valid pixels whose center lat/lon falls within the same grid box, and the number of
201 observations included in that average is recorded. These daily gridded datasets were then averaged to
202 look at statistics on the monthly to seasonal scale.

203 **3.2 Direct Comparison**

204 Once gridding of the data was completed, the datasets were directly compared through analysis of un-
205 paired seasonal AOT and looking at the differences in retrieval numbers. Due to the ability of MAIAC
206 to retrieve AOT over brighter surfaces, it was expected that it would have greater spatial coverage than
207 the operational VIIRS product, particularly in areas of sparse vegetation.

208 **3.2.1 Data coverage**

209 Seasonal averages of AOT from MAIAC and VIIRS and the total number of retrievals per grid were
210 analyzed in order to get a sense of the differences in coverage, and gain insight into the retrieval strategy
211 and cloud screening of each algorithm. Figure 2 provides a look at the average of AOT (top) and
212 number of retrievals per grid (bottom) per season for each dataset. MAIAC has greater coverage and
213 more retrievals than VIIRS particularly across the western half of the CONUS. MAIAC coverage is
214 nearly complete during the summer and fall seasons, save for some inland water bodies and regions such
215 as Great Salt Flats (UT) and White Sands (NM), while VIIRS is not able to retrieve over the bright
216 surfaces that make up a large portion of the western U.S. This disparity in coverage is seen across all
217 seasons with the differences being greater during winter and spring due to seasonal phenology. There are
218 some similarities however; for instance during winter when neither MAIAC or VIIRS retrieve enough to
219 populate grids over the northernmost sections of the U.S. or the high altitude regions of the inter-
220 mountain west. The reason for this is likely a combination of the solar zenith angle limits placed on
221 good quality data and near-constant snow cover in these regions during the cold season.

222 In terms of actual AOT values, Figure 2c highlights some differences between MAIAC and VIIRS.
223 While the spatial patterns are very similar between the two, VIIRS tends to retrieve slightly higher AOT
224 over many regions. Over urban areas or mountainous terrain, this difference can be quite large and is
225 noticeable in many seasons. In the springtime months, VIIRS AOT is also higher in the upper Mid-west
226 and Great Lakes region where melting snow is likely contaminating the pixels leading to a poor
227 retrieval. These anomalies associated with sub-pixel snow have since been addressed in the operational
228 VIIRS algorithm.

229 Looking collectively at the results of this comparison, there are some features present in multiple
230 seasons which emphasize the differences between the two algorithms and their pixel selection strategy.
231 The underlying surface reflectance plays an important role in coverage of both datasets. MAIAC has
232 shown the ability to retrieve AOT over the bright and soil dominated surfaces that are present across

233 much of the western U.S., while VIIRS is only able to retrieve over darker or vegetated regions. This is
234 also a problem in regions with high agricultural activity, such as the Lower Mississippi River Basin
235 where fallow land prevents VIIRS from consistently retrieving AOT in all seasons besides the primary
236 growing season (JJA). However surface reflectance alone cannot account for the differences in
237 retrievals seen in many other parts of the US throughout the year.

238 **3.2.2 Cloud Screening**

239 In an effort to understand the difference in coverage and to determine how the cloud masks are
240 performing, data from MAIAC and VIIRS were collocated with the CALIOP instrument aboard the
241 CALIPSO satellite. First, the two cloud masks are converted to a binary mask with either a ‘clear’ or
242 ‘cloudy’ designation. All datasets are subsetted to regions of overlap, after which the closest
243 MAIAC/VIIRS pixel to the CALIOP profile is found using a modified version of the nearest neighbor
244 approach utilized in similar comparison studies [*Heidinger et al., 2012; Kopp et al., 2014*]. Here we use
245 a time window of 10 minutes centered on the CALIOP observation time in order to avoid cases where
246 clouds detected by CALIOP have moved out of the MAIAC/VIIRS field of view. A maximum allowed
247 distance of one pixel width is used to ensure that the closest pixel is indeed chosen, this is particularly
248 necessary where the CALIOP profile passes from one tile/granule to the next. Collocation results
249 between the cloud masks and CALOP detection were compared and are presented in Table 1 as a
250 confusion matrix.

251 Our first observation from Table 1 is that a considerably higher number of collocations for MAIAC exist
252 than for VIIRS. This is not only due to MAIAC’s increased retrieval numbers but the use of reflectance
253 data from MODIS, which is part of the A-train constellation [*Stephens et al., 2002*] and shares a similar
254 orbit and overpass time with CALIPSO. The VIIRS instrument flies at a slightly higher altitude and

255 therefore has a different orbital track, the consequence of which is a ground track that only coincides
256 closely with the A-train satellites once every few days.

257 To help determine the performance of each set of matchups we look at overall accuracy (Equation 1)
258 along with two additional statistical measures: the True Positive Rate (TPR), and True Negative Rate
259 (TNR) for which the formulas are given in Equations 2 and 3, respectively. The abbreviations used in
260 these equations are noted next to their respective statistics in Table 1. A high TPR value indicates that
261 the cloud mask is able to limit the number of false negatives (type II error), which lead to cloud leakage
262 in the resulting product. Conversely, TNR is a measure of how good the cloud mask is at reducing the
263 number of false positives (type I error); these false alarms can reduce the number of high quality
264 retrievals and introduce sampling biases.

$$265 \quad Accuracy = \frac{TP + TN}{TP + TN + FN + FP}$$

266

$$267 \quad TPR = \frac{TP}{TP + FN}$$

268

$$269 \quad TNR = \frac{TN}{TN + FP}$$

270

271 Overall accuracy of the both the MAIAC cloud mask (MCM) and the VCM were found to be identical
272 (Table 1), but while the overall accuracy for the two cloud masks may be comparable, the errors
273 observed were dissimilar. The TPR and TNR metrics highlight the different types of errors associated
274 with each cloud mask. For instance, TPR for the MCM during this period is 96%, meaning that less
275 than 5% of cloudy pixels were incorrectly designated as clear, while the TNR for MAIAC is only 72%,
276 leaving over a quarter of the clear pixels as determined by CALIOP out of the AOT processing chain

277 due to the supposition they are cloudy. Monthly statistics for MAIAC show there is some seasonality to
278 the TNR since it does not fall below 71% for much of the year except during summer (JJA) when it is in
279 the 63%-66% range. The VCM displays a smaller difference between its error types with a TPR of 82%
280 and a TNR of 92%, and a more limited seasonal dependence. These results show that VIIRS is able to
281 strike a better balance between the Type I and Type II errors, while MAIAC's strength is its ability to
282 greatly reduce false negatives in the AOT record, thereby reducing bias.

283 In terms of these Type I errors, since the MCM operates at both the block and pixel level, it is possible
284 that diurnal convection produces sufficient cloud cover to cause the covariance between that block and
285 the clear-sky reference image to decrease to the point that it is deemed cloudy. Likewise, cumulus cloud
286 fields common over land during this season may be enough to trigger a cloudy designation for that pixel
287 from MAIAC, while the very narrow field of view of the CALIOP sensor may pass between these small
288 clouds leading to a conflicting collocation. Such instances of small clouds and sub-pixel clouds pose
289 problems for all types of cloud masks produced by passive sensors.

290 Seasonal statistics (Fig. 2) showed that MAIAC has a significantly greater number of high quality
291 retrievals than VIIRS in many U.S. regions, even those where the surface is not bright enough to keep
292 the algorithm from performing the retrieval. This would imply that either MAIAC is opting to retrieve
293 AOT in unfavorable conditions (presence of clouds/snow, etc.) or that VIIRS is failing to retrieve at a
294 high quality over these areas. The results of the matchups with CALIPSO seem to suggest the later, as
295 the MCM is being conservative in determining which pixels are cloud-free. Therefore, cloud screening
296 is not thought to be a substantial driver behind the differences in retrieval numbers; however other limits
297 placed on AOT retrievals within the algorithms may be playing a part in the spatial coverage.

298 Some recent preliminary analysis by the VIIRS Aerosol team into gaps in AOT over the CONUS has
299 shown that the most probable cause for the reduced number of high quality IP retrievals is the limited

300 AOT range (0 to 2); and more precisely in this case, the lower bound of zero. Unlike VIIRS, which
301 excludes the candidate pixel if the minimum residual corresponds to an AOT less than 0, MAIAC does
302 not reject pixels whose surface reflectance falls below the expected value when computed with an AOD
303 equal to 0. This happens on the occasion that the surface has changed significantly, or that the previous
304 surface characterization is not correct. In the event this situation occurs, MAIAC reports an AOT of zero
305 and then focuses on correcting the surface characterization with the next observation.

306 Large areas of missing AOT in VIIRS granules can be found in regions where the atmosphere is free of
307 clouds or visible aerosols, meaning that the AOT is too small (negative) to be given a quality level high
308 enough to be reported by the algorithm. This phenomenon is most prevalent in winter and spring when
309 the AOT loading is small, and tends to be enhanced when the surface is sparsely vegetated and being
310 viewed from the backscattering direction. In the recent VIIRS aerosol validation analysis performed by
311 *Huang et al.*, (2016) it was shown that VIIRS is often negatively biased during the period from late fall
312 to early spring. Additionally, *Liu et al.*, (2013) showed that VIIRS AOT tends to underestimate AOT
313 when the surface is soil dominated. These two conclusions from previous validation studies support the
314 notion that VIIRS has a tendency to retrieve more negative AOT when certain seasonal, geometric, and
315 surface conditions are present, which can lead to relatively large areas with limited to no retrievals.

316 **3.2.3 Collocated retrievals of AOT**

317 As noted in the previous section, VIIRS and MAIAC tend to characterize the spatial patterns of seasonal
318 AOT in similar ways. It also appears that MAIAC is generally a bit lower when compared to VIIRS,
319 especially in the warm season. Observations collocated in time and space are needed to make sure that
320 these two AOT products are being compared to one another under the same conditions. Therefore, the
321 gridded data are filtered so that only days when both algorithms have enough retrievals to populate the
322 grid cell are used in the analysis. Figure 3 presents the results of this collocation for the spring and

323 summer seasons when the differences between the two are greatest. While there is better agreement
324 between MAIAC and VIIRS across much of the domain, the same trend of elevated AOT from VIIRS
325 over the larger urban areas persists. Summer is the season with the highest disparity between the two
326 algorithms, when a widespread difference between VIIRS and MAIAC is seen in the eastern half of the
327 domain. In Figure 3d, this difference is shown to be predominately ± 0.1 or less; however there are small
328 isolated pockets of larger bias up to 0.5. In other seasons, there is little systematic disagreement between
329 the two with the exception of some high AOT from VIIRS over Montana and the Dakotas during the
330 spring season. This discrepancy between the two could be a result of cloud contamination, or differences
331 in surface characterization.

332 Those areas where VIIRS is significantly higher than MAIAC are likely caused by the underlying
333 surface since many of these anomalies are predominately located over heavily urbanized areas and
334 mountainous terrain. There are also smaller differences which are not as persistent but cover larger
335 areas. An example of this can be seen in the summer season where VIIRS AOT in the eastern half of the
336 U.S. is ubiquitously higher than MAIAC. Aerosol type and concentration can be widely different based
337 on region, and problems characterizing these differences may be caused by certain underlying aspects of
338 the aerosol algorithms.

339 One such component of the algorithms that could be responsible for the regional contrast is the different
340 aerosol models used to retrieve AOT. MAIAC uses a dynamic model where physical parameters can
341 change based on the magnitude of AOT. Volumetric concentrations of the fine and coarse particles can
342 also be varied, thereby allowing for a wider range of size parameter to be simulated. In addition,
343 MAIAC uses a background aerosol model that is tuned regionally based on AERONET optical thickness
344 measurements. As a global product, VIIRS on the other hand uses five predefined aerosol models which
345 have bimodal size distributions and static volumetric concentration parameters for each of the models
346 and both particle sizes. Although not related to the aerosol models themselves, VIIRS also uses a

347 globally constant surface reflectance ratio to compare against the retrieved reflectance. This lack of
348 accounting for such variations in surface type was discussed by *Liu et al.*, (2013) as a potential source of
349 regional bias in the AOT retrievals. In that analysis it was also found that VIIRS is biased high in the
350 Eastern U.S. when compared to both AERONET and MODIS. Together, these differences in aerosol
351 models and surface characterization are capable of producing the regional variations in AOT retrieved
352 from MAIAC and VIIRS.

353 **3.3 Validation of products**

354 **3.3.1 Comparison with AERONET AOT**

355 In general, AOT from MAIAC and VIIRS compare well to one another, however there are differences
356 and it is difficult to get a sense of which exhibits the higher level of accuracy without an ‘unbiased’
357 dataset to compare against. Measurements from AERONET sun photometers have been used for this
358 purpose for many of the satellite derived aerosol products since the network’s inception [*Chu et al.*,
359 2002; *Kahn et al.*, 2005, *Liu et al.*, 2013]. Most recently, in a manuscript by *Huang et al.*, (2016) it was
360 found using AERONET level 2 data that the VIIRS IP product has a global bias of 0.04. To determine
361 the bias of the AOT produced by the two algorithms in question over our domain, we construct a set of
362 matchups with AERONET level 2 data using the original datasets at their nominal resolution. *Petrenko*
363 *et al.*, (2012) outlined a system for subsetting data from spaceborne sensors based on the location of
364 ground-based sensors such as AERONET. This same process of matching our datasets with AERONET
365 is used here, where all good quality retrievals within 27.5 km of the AERONET site are selected. As
366 part of the matchup criteria, at least 20% of the total number of possible pixels within this circle are
367 needed along with a minimum of 4 AERONET measurements over the time period of one hour centered
368 on the satellite overpass time are required. All pixels found to meet these requirements are averaged
369 together, as are all ground measurement that fall in the time window.

370 Figure 4 shows the scatter plots constructed using the AERONET matchups with VIIRS and MAIAC.
371 For all data matchups, VIIRS has a noticeable high bias which is pervasive at $AOT < 0.04$, and a
372 moderate correlation of 0.64 with AERONET. However, a VIIRS positive bias of 0.043 compares well
373 with the results of the global matchups presented in Huang et al., (2016). MAIAC on the other hand is
374 highly correlated (0.82) with AERONET and exhibits only a slight negative bias when compared with
375 AERONET. The greater number of MAIAC matchups is further evidence of its coverage and ability to
376 retrieve over the brighter surfaces over which many AERONET stations in the western U.S. are located.
377 In Figure 5, we highlight the dependence of the AOT bias on the magnitude of AOT by plotting the
378 differences between VIIRS and AERONET at 25 AOT bins of increasing size. The typical error
379 (median of all matchup errors) is often less than ± 0.05 with the exception of the strong negative bias for
380 both products during times of high aerosol loading, with MAIAC having slightly greater bias as AOT
381 increases. The spread of VIIRS errors however is much greater than those for MAIAC as evidenced by
382 the larger quartile ranges in most bins and the much higher maximum errors seen at low AOT.

383 Aerosol type is also an important consideration when evaluating the AOT retrievals since the chosen
384 aerosol model determines the spectral dependence of AOT. This spectral AOT can act as a proxy for
385 particle size, and the Angstrom Exponent (AE) is often used to qualitatively describe this spectral
386 dependence [Angstrom, 1929]. AE for coarse mode particles such as dust tend to be < 1 , while finer
387 particles produced from urban pollution or biomass burning are associated with AE values > 2 [Reid et
388 al., 1999; Schuster et al., 2006]. AERONET provides AE for multiple wavelength pairs and can be used
389 to determine if the retrieval errors from MAIAC or VIIRS are dependent on particle size. Figure 6
390 provides a look at how each algorithm performs across the range of particle sizes. The color coding of
391 the individual matchups is based on the AOT retrieved by AERONET. There is evidence of the larger
392 positive biases present and previously discussed in the VIIRS data which is limited to low-to-moderate
393 loading of finer particles. MAIAC meanwhile has very limited bias and dependence on particle size as

394 shown by the regression line. MAIAC however does have some issues retrieving accurately during high
395 aerosol loading of coarse or mixed particle sizes (AE between 0.5 and 1.75). Figure 6 also reaffirms the
396 results portrayed in Figure 4, however it shows that the larger biases tend to occur when the aerosol
397 particle size is large, or when the concentration of coarse and fine particles is mixed. Both algorithms
398 appear to perform quite well during cases of smoke or urban pollution.

399 While not analyzed directly here for reasons stated in Section 1, the demonstrated performance of the
400 MODIS aerosol product is useful for providing extra context. A study from 2013 by Levy et al. details
401 the performance of the MODIS Collection 6 algorithm and specifically section 4.4 outlines the MODIS
402 Dark Target (DT) algorithm. Results for MAIAC shown here in Figures 4 & 5 compare well with the
403 MODIS algorithm (Figure 11 in Levy et al.) over land with similar levels of accuracy and precision. It is
404 important to note however that the Levy et al. study used global DT data, whereas MAIAC retrieves
405 over both dark and bright surfaces and is constrained to the CONUS region in our analysis.

406 **3.3.2 Dependence of AOT on Viewing Geometry and Surface Reflectance**

407 In an attempt to ascertain which conditions might cause biases in the AOT retrievals, we look at how
408 they are impacted by changing viewing geometry and surface brightness. Only data points where both
409 VIIRS and MAIAC are matched with AERONET observations are used for this purpose, resulting in a
410 dataset of 1034 matchups. Viewing geometry dependence is determined using the following 3
411 parameters: viewing zenith angle; relative azimuth angle; and scattering angle. The AOT biases are
412 separated into bins using 5 degree increments and plotted as a function of increasing angle. The results
413 are shown in panels a, b, and c of Figure 7.

414 In terms of viewing angle, both algorithms produce matches that are well distributed across the range of
415 angles with VIIRS having greater range as a result of the increased swath width over MODIS. MAIAC
416 has very little viewing angle dependence, and has a minimal amount of a negative bias. VIIRS has some

417 viewing angle dependence with positive biases at-nadir that approach zero for larger VZA. The number
418 of matchups are not as uniform for RAA, as both MAIAC and VIIRS have a bimodal distribution of
419 angles with limited number of matches near 90° . MAIAC has some small dependence on RAA but
420 biases are generally low except for the $80\text{-}110^\circ$ range and near the extremes of 0° and 180° where
421 matchups are very scarce. VIIRS AOT starts out with positive bias where strong back-scattering is
422 occurring ($\text{RAA} < 50^\circ$) with little dependency, however bias increases dramatically as the relative
423 azimuth angle approaches 180° . It is worth noting that a limited amount of VIIRS matchups are
424 available at $\text{RAA} > 140^\circ$, which is a range with both high bias and variability. Both algorithms have
425 some bias dependence on scattering angle. MAIAC biases are within 0.02 of the zero line for smaller
426 scattering angles, but the negative bias continues to get larger once SCA surpasses 140° . VIIRS also
427 has a small negative bias which then becomes positive as scattering angle increases.

428 Figure 7d shows the dependence of the two algorithms in terms of the MAIAC surface reflectance which
429 is binned at intervals of 0.005. Minimal errors are observed for both datasets over dark surfaces up to a
430 reflectance of 0.06, after which the algorithms start slowly trending in different directions. The error
431 becomes larger for VIIRS once the surface reflectance reaches 0.12, while MAIAC dependence on
432 surface reflectance reverses after this point. The brighter surfaces also appear to cause increased
433 fluctuation in bias for both of the algorithms

434 As noted previously, there is some dependence on sun-sensor geometry for both of the algorithms
435 analyzed here. Notably, there is a large difference in the level of dependence between retrievals in the
436 back-scattering direction ($\text{RAA} < 90^\circ$) and the forward-scattering direction ($\text{RAA} > 90^\circ$) for VIIRS. The
437 two algorithms also drift away from the zero line in opposite directions for scattering angles greater than
438 100° . Due to the anisotropy of surface reflectance for many land targets, this change in viewing direction
439 can lead to changes in the perceptible brightness of the surface, a phenomenon known as directional
440 scattering. This effect causes an apparent brightening of the surface when viewed from in the back-

441 scattering direction, and some dimming in the forward-scattering direction [Roujean, 1992]. MAIAC,
442 through its use of the BRDF when retrieving AOT, attempts to account for and mitigate these effects.
443 Based on the results in Figure 7d, it appears as though it is able to remove much of this dependence;
444 VIIRS meanwhile, because of the assumption of a Lambertian surface, produces AOT with higher
445 biases.

446 To see how each algorithm handles these changes the matchups for surface reflectance have been further
447 stratified based on the scattering direction (using RAA of 90° as a separator). The resulting biases and
448 histograms for both directions are given in Figure 8. VIIRS dependencies are similar regardless of the
449 scattering direction, although errors are markedly higher in the forward-scattering direction for brighter
450 surfaces. On the other hand, the dependency for MAIAC does look quite different depending on the
451 scattering direction. MAIAC errors are near zero over dark surfaces in the back-scattering direction, yet
452 quickly become negative as the surface gets brighter. In the forward-scattering direction, a rather
453 consistent negative bias around -0.05 is found until surface reflectance surpasses 0.12, when it becomes
454 more varied. Comparing these two panels to Figure 6d, we see that the back-scattering retrievals tend to
455 dominate the overall signal due to nearly two-thirds of the retrieval matchups falling within this relative
456 azimuth range; with the only exception being the bright surfaces where MAIAC has few valid retrievals.
457 The histograms also show that MAIAC has some offset in the surface reflectance of its retrievals in both
458 directions when compared to VIIRS. This is likely a result of including the BRDF in its retrieval strategy
459 which accounts for the effects of sun and satellite geometry thereby reducing the brightness in the
460 backward direction and increasing it in the forward direction.

461 **3.3.3 Sources of Bias**

462 Matchups of MAIAC and VIIRS with AERONET data in the U.S. and surrounding areas have shown
463 that biases are present that are angular dependent. MAIAC dependencies are less pronounced than
464 VIIRS, but a negative association with geometric surface attributes does exist. *Lyapustin et al., (2011)*

465 showed that SRC does vary slightly with viewing geometry, and that the use of an average SRC value
466 will cause the algorithm to overestimate surface reflectance in the forward direction and vice-versa for
467 back-scattering geometries. This reduced brightening in the backward direction and increase in the
468 surface reflectance in the forward scattering direction relative to VIIRS is evident in the histogram
469 offsets seen in Figure 8.

470 The consequence of this would be an underestimated AOT in the forward-scattering direction, and
471 overestimation in the back-scattering direction, however we only find a consistent negative bias in the
472 forward direction. In the back-scattering direction, the surface tends to be brighter due to reduced
473 shadowing and lower aerosol backscattering compared to the forward-scattering direction. This can
474 cause the sensitivity of the TOA reflectance to AOT to decrease, leading to higher uncertainty of AOT
475 in the back-scattering direction. This combined with the limited amount of MAIAC matchups with a
476 high surface reflectance in the back-scattering direction are likely leading to the larger, variable errors
477 over bright surfaces.

478 Previous global validation studies have focused on VIIRS Aerosol products [*Liu et al.*, 2013 (EDR
479 only); *Huang et al.*, 2016 (EDR and IP)] and have shown that a slight positive bias is observed in AOT
480 over land. As is shown in this analysis, *Liu et al.*, (2013) also found a similar dependence in the EDR
481 data in relationship to viewing zenith angle over land as is shown in this paper, although errors were
482 found to be larger in this case. This is not surprising as more noise is expected in the pixel-level IP AOT
483 data, which does not have the benefit of aggregation and further screening. Even with that in mind, the
484 level of bias seen in this study for VIIRS products is concerning since data at this product level is useful
485 to the air quality community who require highly accurate data for their applications. Therefore, a brief
486 attempt was made to uncover additional sources of bias to those already established by previous studies.

487 Recall from section 3.2 that urban ‘hotspots’ of AOT were consistently present over medium to large
488 cities across the U.S. in all seasons (more so in warm seasons). A fair amount of AERONET sites that
489 are not surrounded by bright or soil-dominated surfaces in the U.S. are located in or near these urban
490 areas, meaning that some of the bias may be attributed to these sites. In fact, of those matchups which
491 exhibit excessive positive bias (> 0.1), 65% of them are associated with a handful of sites located in Los
492 Angeles or Houston, two large and highly urbanized cities. Over 85% of the highly biased matchups
493 (20% of all matchups) originate from AERONET sites located in a major metro area. When looking at
494 viewing geometry values where large biases are seen, we notice a considerable number of those
495 AERONET sites also being in select urban areas, while sites with lower biases tend to be more random.
496 This suggests that a sizable portion of the large biases and dependencies on viewing geometry in this
497 domain may be due to a lack of accuracy over urban areas and that viewing geometry is an intensifier of
498 those biases.

499 **4. AOT case studies**

500 Up to this point, the geographic inspection of the AOT products from MAIAC and VIIRS have been
501 contained to seasonally gridded AOT. In an attempt to observe and verify some of the findings from the
502 bias analysis, a look at individual cases at the products’ native resolution are presented below. This
503 allows for qualitative comparison of the two products independent of the AERONET matchups which,
504 with respect to VIIRS, were found to be heavily influenced by an urban bias. Two cases; one with a
505 large area of smoke present over the northwestern U.S. and a more typical late-summer AOT case in the
506 eastern half of the country were chosen. Careful attention was paid to make certain that the Aqua and
507 Suomi-NPP overpass times for the selected date were close together (< 20 min) so valid spatial
508 comparisons could be made.

509 **4.1 High AOT case**

510 In 2013, a few large historical wildfires took place in North America with one such fire being the Rim
511 fire, which started on August 17th near Yosemite National Park and burned for over two months. Figure
512 9 shows a VIIRS true-color image over the Western U.S. from August 25th along with AOT from VIIRS
513 and MAIAC. The two products agree well over regions where both have retrieved AOT, however
514 differences do exist. VIIRS IP AOT is higher over the thickest parts of the smoke plume and is noisier,
515 however this is expected since it is a pixel-level product while the MAIAC AOT has the advantage of
516 using gridded MODIS reflectance, and much of the information used to perform the retrieval is supplied
517 from processing at the block-level.

518 Just as the analysis in section 3 showed, VIIRS coverage over brighter surfaces is limited compared to
519 MAIAC, as large sections of Montana, Idaho and Wyoming lack any high quality retrievals. However
520 VIIRS does retrieve more of the smoke in northern Idaho. The missing MAIAC retrievals in the far
521 upper right section of the image are a result of it being outside MAIAC's North American processing
522 domain. There are also smaller rectangular holes in the MAIAC data near the center of the image which
523 are a product of the block-level SRC retrieval that takes place within the aerosol retrieval. In some
524 cases, SRC may not be retrieved or updated due to cloudiness. This causes AOT to not be retrieved over
525 the brighter surfaces within that block (25 km x 25km).

526 **4.2 Moderate AOT case**

527 Given that strong AOT bias dependencies exist in both the viewing geometry and AOT itself, a second
528 case representing a more moderate aerosol loading scenario was investigated. Figure 10 includes the
529 true-color image and AOT maps from VIIRS and MAIAC on Sept. 5th, 2013 over the Mid-western and
530 Mid-Atlantic states. In contrast to the previous example, the spatial coverage of VIIRS is much closer to
531 MAIAC in this case due to a majority of the surface being dark. The exception here is over inland water
532 bodies such as the Great Lakes where VIIRS currently does not retrieve AOT. Once again, the two

533 products characterize the spatial variation in AOT in similar ways. Over much of the Ohio River valley,
534 where an area of haze exists, the two algorithms produce results that are very alike, although VIIRS
535 AOT is slightly higher in the vicinity of clouds in northern Illinois. VIIRS is also significantly higher
536 over the Chicago and St. Louis urban areas which are circled in black, lending credibility to the theory
537 that VIIRS is often biased high over cities. No AERONET sites are located in Chicago, but one is
538 located in downtown St. Louis, where data shows that VIIRS is biased high by 0.05 while MAIAC has a
539 bias of -0.11. There are also areas where VIIRS is retrieving slightly higher AOT in a more uniform
540 manner. The clearest example of this is in the Mid-Atlantic where VIIRS is retrieving AOTs which are
541 around 0.05 higher than MAIAC. A similar pattern is also visible over a region stretching from Lake
542 Michigan into Ohio and Pennsylvania.

543

544 **5. Conclusions**

545 This study was undertaken to assess the utility of the MAIAC algorithm for retrieving aerosol
546 information from a passive satellite sensor through a comparison with the aerosol products from VIIRS
547 and ground-based sun photometers. With these data sets as benchmarks, we were able to evaluate the
548 spatial coverage and accuracy of the MAIAC AOT product. Using data gridded to 0.25 degrees, we
549 found that MAIAC is capable of providing retrievals over a varied set of surface types, including the
550 bright and soil dominated surfaces which restrict the coverage of the common dark-target only
551 algorithms (VIIRS, MODIS). The number of valid high-quality retrievals MAIAC produces is also
552 greater, leading us to evaluate the cloud mask performance of both algorithms through matchups with
553 CALIOP. Those matchups showed that both MAIAC and VIIRS had similar accuracy, however we
554 found MAIAC to be more conservative in its assignment of clear-sky pixels. When compared directly
555 with VIIRS, MAIAC produces AOT values that on average are 0.017 lower than VIIRS during 2013.

556 There is large seasonality however, with minor differences for winter and fall, and larger separation seen
557 in the summer season.

558 In order to conduct a more robust accuracy assessment including the dependence of the algorithms on
559 viewing geometry and surface reflectance, both datasets were also evaluated against AERONET Level 2
560 AOT. MAIAC showed little dependence on viewing zenith, however there was some negative
561 association with the scattering angle and the brightness of the surface. VIIRS showed negative
562 association with viewing angle, but was positive with scattering angle and surface reflectance. Biases as
563 a function of surface reflectance were further stratified based on scattering direction because of the
564 differences in errors seen with both products. Trends in VIIRS bias as a function of surface reflectance
565 were not greatly affected by scattering direction, although overall errors were larger in the forward-
566 scattering direction. Analysis of MAIAC showed that it only has strong dependence on surface
567 reflectance when the surface is viewed in the back-scattering direction.

568 The results of this bias analysis coincided well with the initial investigations of the MAIAC algorithm.
569 The results after studying the VIIRS biases with respect to scattering direction however were not
570 consistent with previous validation studies; therefore a closer look was taken at those highly biased
571 matchups. It was found that urban backgrounds may be causing, or at least intensifying the positive bias
572 seen in VIIRS AOT. Overall, the MAIAC algorithm has shown the ability to perform well over the
573 North American region with a high level of accuracy given its spatial resolution. Global analysis over a
574 longer time period will be needed to make certain that the product(s) are robust and meet the levels of
575 accuracy needed for aerosol monitoring.

576

577 **Acknowledgements.** The work outlined in this manuscript was supported by the NOAA JPSS program
578 office and NASA as part of a GEO-CAPE aerosol science study. In addition, the authors would like to

579 recognize the following for their support throughout the study: I. Laszlo, H. Liu along with the entire
580 NOAA/NESDIS/STAR Aerosol team. We also thank the AERONET principle investigators and their
581 staff for the establishment and maintenance of the North American sites used as part of this
582 investigation. VIIRS aerosol products are available at NOAA's Comprehensive Large Array-Data
583 Stewardship System (CLASS, <http://www.class.ngdc.noaa.gov/>) MAIAC Aerosol products can be
584 accessed through at the NASA ftp site:
585 <ftp://maiac@dataportal.nccs.nasa.gov/DataRelease/NorthAmerica>. The AERONET data used in this
586 study is publically available from the AERONET team at the NASA GFSC site
587 (<http://aeronet.gsfc.nasa.gov/>). Data from CALIPSO were obtained from the NASA Langley Research
588 Center Atmospheric Science Data Center (ASDC). The contents of this manuscript are solely the
589 opinions of the authors and do not constitute a statement of policy, decision, or position on behalf of
590 NOAA or the U.S. Government.

591

592

593

594 **References**

- 595 Al-Saadi, J., Szykman, J., Pierce, R. B., Kittaka, C., Neil, D., Chu, D. A., & Fishman, J. (2005).
596 Improving national air quality forecasts with satellite aerosol observations. *Bulletin of the American*
597 *Meteorological Society*, 86(9), 1249-1261.
- 598 Ångström, A. (1929). On the atmospheric transmission of sun radiation and on dust in the
599 air. *Geografiska Annaler*, 11, 156-166.

600 Chu, D. A., Kaufman, Y. J., Ichoku, C., Remer, L. A., Tanré, D., & Holben, B. N. (2002). Validation
601 of MODIS aerosol optical depth retrieval over land. *Geophysical research letters*, 29(12), MOD2-1.

602 Fishman, J., L. T. Iraci, J. Al-Saadi, Kelly V. Chance, F. Chavez, M. Chin, P. Coble, 2012. “The
603 United States’ Next Generation of Atmospheric Composition and Coastal Ecosystem Measurements:
604 NASA’s Geostationary Coastal and Air Pollution Events (GEO-CAPE) Mission.” *Bulletin of the
605 American Meteorological Society* 93 (10) (October): 1547–1566. doi:10.1175/bams-d-11-00201.1.

606 Frey, R. A., Ackerman, S. A., Liu, Y., Strabala, K. I., Zhang, H., Key, J. R., & Wang, X. (2008).
607 Cloud detection with MODIS. Part I: Improvements in the MODIS cloud mask for collection
608 5. *Journal of Atmospheric and Oceanic Technology*, 25(7), 1057-1072.

609 Gao, B. C., & Kaufman, Y. J. (2003). Water vapor retrievals using Moderate Resolution Imaging
610 Spectroradiometer (MODIS) near-infrared channels. *Journal of Geophysical Research:
611 Atmospheres*, 108(D13).

612 Heidinger, A. K., Evan, A. T., Foster, M. J., & Walther, A. (2012). A naive Bayesian cloud-
613 detection scheme derived from CALIPSO and applied within PATMOS-x. *Journal of Applied
614 Meteorology and Climatology*, 51(6), 1129-1144.

615 Holben, B., Vermote, E., Kaufman, Y. J., Tanré, D., & Kalb, V. (1992). Aerosol retrieval over land
616 from AVHRR data-application for atmospheric correction. *Geoscience and Remote Sensing, IEEE
617 Transactions on*, 30(2), 212-222.

618 Holben, B. N., Eck, T. F., Slutsker, I., Tanre, D., Buis, J. P., Setzer, A., & Smirnov, A. (1998).
619 AERONET—A federated instrument network and data archive for aerosol characterization. *Remote
620 sensing of environment*, 66(1), 1-16.

621 Huang, J., S. Kondragunta, I. Laszlo, H. Liu, L. A. Remer, H. Zhang, S. Superczynski, P. Ciren, B.
622 N. Holben, and M. Petrenko (2016), Validation and expected error estimation of Suomi-NPP VIIRS
623 aerosol optical thickness and Ångström exponent with AERONET, *Journal of Geophysical*
624 *Research: Atmospheres*, 121, doi:10.1002/2016JD024834.

625 Holben B., & Petrenko M. (2016). Validation and Expected Error Estimation of S-NPP VIIRS
626 Aerosol Optical Thickness and Angstrom Exponent with AERONET. *Journal of Geophysical*
627 *Research: Atmospheres*, 121, doi:10.1002/2016JD024834.

628 Jackson, J. M., Liu, H., Laszlo, I., Kondragunta, S., Remer, L. A., Huang, J., & Huang, H. C. (2013).
629 Suomi-NPP VIIRS aerosol algorithms and data products. *Journal of Geophysical Research:*
630 *Atmospheres*, 118(22), 12-673.

631 Kahn, R. A., Gaitley, B. J., Martonchik, J. V., Diner, D. J., Crean, K. A., & Holben, B. (2005).
632 Multi-Angle Imaging Spectroradiometer (MISR) global aerosol optical depth validation based on 2
633 years of coincident Aerosol Robotic Network (AERONET) observations. *Journal of Geophysical*
634 *Research: Atmospheres (1984–2012)*, 110(D10).

635 Kaufman, Y. J., Tanré, D., Remer, L. A., Vermote, E. F., Chu, A., & Holben, B. N. (1997).
636 Operational remote sensing of tropospheric aerosol over land from EOS moderate resolution
637 imaging spectroradiometer. *Journal of Geophysical Research: Atmospheres (1984–2012)*, 102(D14),
638 17051-17067.

639 Kopp, T. J., Thomas, W., Heidinger, A. K., Botambekov, D., Frey, R. A., Hutchison, K. D., & Reed,
640 B. (2014). The VIIRS Cloud Mask: Progress in the first year of S-NPP toward a common cloud
641 detection scheme. *Journal of Geophysical Research: Atmospheres*, 119(5), 2441-2456.

642 Lahoz, W. A., Peuch, V. H., Orphal, J., Attié, J. L., Chance, K., Liu, X., ... & Amraoui, L. E. (2012).
643 Monitoring air quality from space: The case for the geostationary platform. *Bulletin of the American*
644 *Meteorological Society*, 93(2), 221-233.

645 Liu, H., Remer, L. A., Huang, J., Huang, H. C., Kondragunta, S., Laszlo, I., & Jackson, J. M. (2014).
646 Preliminary evaluation of S-NPP VIIRS aerosol optical thickness. *Journal of Geophysical Research:*
647 *Atmospheres*, 119(7), 3942-3962.

648 Lyapustin, A., Wang, Y., & Frey, R. (2008). An automatic cloud mask algorithm based on time
649 series of MODIS measurements. *Journal of Geophysical Research: Atmospheres (1984–*
650 *2012)*, 113(D16).

651 Lyapustin, A., Martonchik, J., Wang, Y., Laszlo, I., & Korkin, S. (2011). Multi-
652 Angle implementation of atmospheric correction (MAIAC): 1. Radiative transfer basis and look-up
653 tables. *Journal of Geophysical Research: Atmospheres (1984–2012)*, 116(D3).

654 Lyapustin, A., Wang, Y., Laszlo, I., Kahn, R., Korkin, S., Remer, L., & Reid, J. S. (2011). Multi-
655 Angle implementation of atmospheric correction (MAIAC): 2. Aerosol algorithm. *Journal of*
656 *Geophysical Research: Atmospheres (1984–2012)*, 116(D3).

657 Lyapustin, A. I., Wang, Y., Laszlo, I., Hilker, T., Hall, F. G., Sellers, P. J., & Korkin, S. V. (2012).
658 Multi-angle implementation of atmospheric correction for MODIS (MAIAC): 3. Atmospheric
659 correction. *Remote Sensing of Environment*, 127, 385-393.

660 Lyapustin, A., M. J. Alexander, L. Ott, A. Molod, B. Holben, J. Susskind, and Y. Wang (2014),
661 Observation of mountain lee waves with MODIS NIR column water vapor, *Geophysical Research*.
662 *Letters.*, 41, doi:10.1002/2013GL058770

663 NOAA-NESDIS (2014), Joint Polar Satellite System (JPSS) Program Level 1 Requirements
664 Document Supplement JPSS-REQ-1002. Version 2.10 [Retrieved from
665 http://www.jpss.noaa.gov/assets/pdfs/technical_documents/level_1_requirements_supplement.pdf]
666 NRC (2007): Earth Science and Applications from Space: National Imperatives for the Next Decade
667 and Beyond. The National Academies Press, 400 pp.

668 Petrenko, M., Ichoku, C., & Leptoukh, G. (2012). Multi-sensor aerosol products sampling system
669 (MAPSS). *Atmospheric Measurement Techniques*, 5(5), 913-926.

670 Ramanathan, V. C. P. J., Crutzen, P. J., Kiehl, J. T., & Rosenfeld, D. (2001). Aerosols, climate, and
671 the hydrological cycle. *Science*, 294(5549), 2119-2124.

672 Reid, J. S., Eck, T. F., Christopher, S. A., Hobbs, P. V., & Holben, B. (1999). Use of the Ångström
673 exponent to estimate the variability of optical and physical properties of aging smoke particles in
674 Brazil. *Journal of Geophysical Research: Atmospheres*, 104(D22), 27473-27489.

675 Roujean, J. L. (1992). for the Correction of Remote Sensing Data. *Journal of geophysical*
676 *research*, 97(D18), 20-455.

677 Schuster, G. L., Dubovik, O., & Holben, B. N. (2006). Angstrom exponent and bimodal aerosol size
678 distributions. *Journal of Geophysical Research: Atmospheres*, 111(D7).

679 Smirnov A., B.N.Holben, T.F.Eck, O.Dubovik, and I.Slutsker, 2000: Cloud screening and quality
680 control algorithms for the AERONET database, *Rem.Sens.Env.*, **73**, 337-349.

681 Stephens, G. L., Vane, D. G., Boain, R. J., Mace, G. G., Sassen, K., Wang, Z., ... & CloudSat
682 Science Team, T. (2002). The CloudSat mission and the A-Train: A new dimension of space-based
683 observations of clouds and precipitation. *Bulletin of the American Meteorological Society*, 83(12),
684 1771-1790.

685 Tanré, D., Kaufman, Y. J., Herman, M., & Mattoo, S. (1997). Remote sensing of aerosol properties
 686 over oceans using the MODIS/EOS spectral radiances. *Journal of Geophysical Research:*
 687 *Atmospheres (1984–2012)*, 102(D14), 16971-16988.

688 Vaughan, M. A., Young, S. A., Winker, D. M., Powell, K. A., Omar, A. H., Liu, Z., & Hostetler, C.
 689 A. (2004, November). Fully automated analysis of space-based lidar data: An overview of the
 690 CALIPSO retrieval algorithms and data products. In *Remote Sensing* (pp. 16-30). International
 691 Society for Optics and Photonics.

692 Vermote, E. F., & Kotchenova, S. (2008). Atmospheric correction for the monitoring of land
 693 surfaces. *Journal of Geophysical Research: Atmospheres (1984–2012)*, 113(D23).

694 Wang, J., & Christopher, S. A. (2003). Inter-comparison between satellite-derived aerosol optical
 695 thickness and PM_{2.5} mass: implications for air quality studies. *Geophysical research*
 696 *letters*, 30(21).

697 Winker, D. M., Vaughan, M. A., Omar, A., Hu, Y., Powell, K. A., Liu, Z, Hunt, W. H., Young, S. A. (2009).
 698 Overview of the CALIPSO mission and CALIOP data processing algorithms. *Journal of Atmospheric and*
 699 *Oceanic Technology*, 26(11), 2310-2323.

700

701 **Tables**

702 Table 1. Confusion matrix showing the designation of pixels from each cloud mask associated with the
 703 two algorithms compared with information on clouds from CALIPSO lidar taken as the “truth” datasets.
 704 The abbreviations in parenthesis note the location of the following test outcomes for both sets of data:
 705 True Positive (TP); False Positive (FP); False Negative (FN); and True Negative (TN).

		VIIRS		MAIAC	
		Cloudy	Clear	Cloudy	Clear
CALIPSO	Cloudy	65079 (TP)	14479 (FN)	1055111	40781
	Clear	4129 (FP)	47298 (TN)	235293	605130

Accuracy	86%	86%
----------	-----	-----

706

707

708

709

710

711

712

713

714

715

716

717

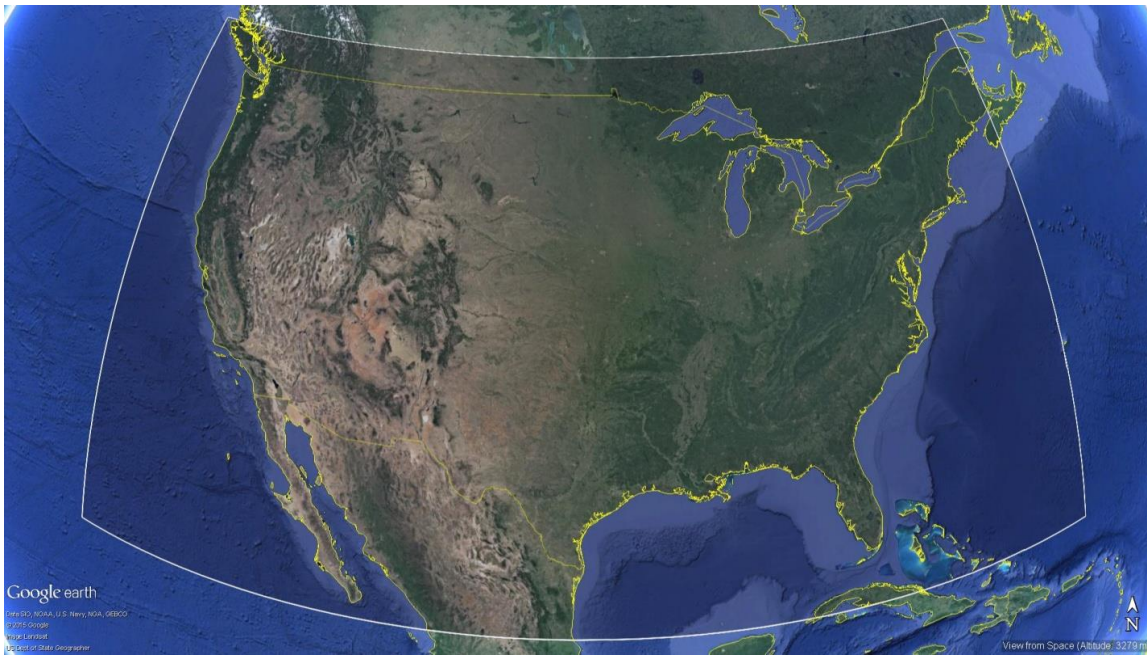
718

719

720

721

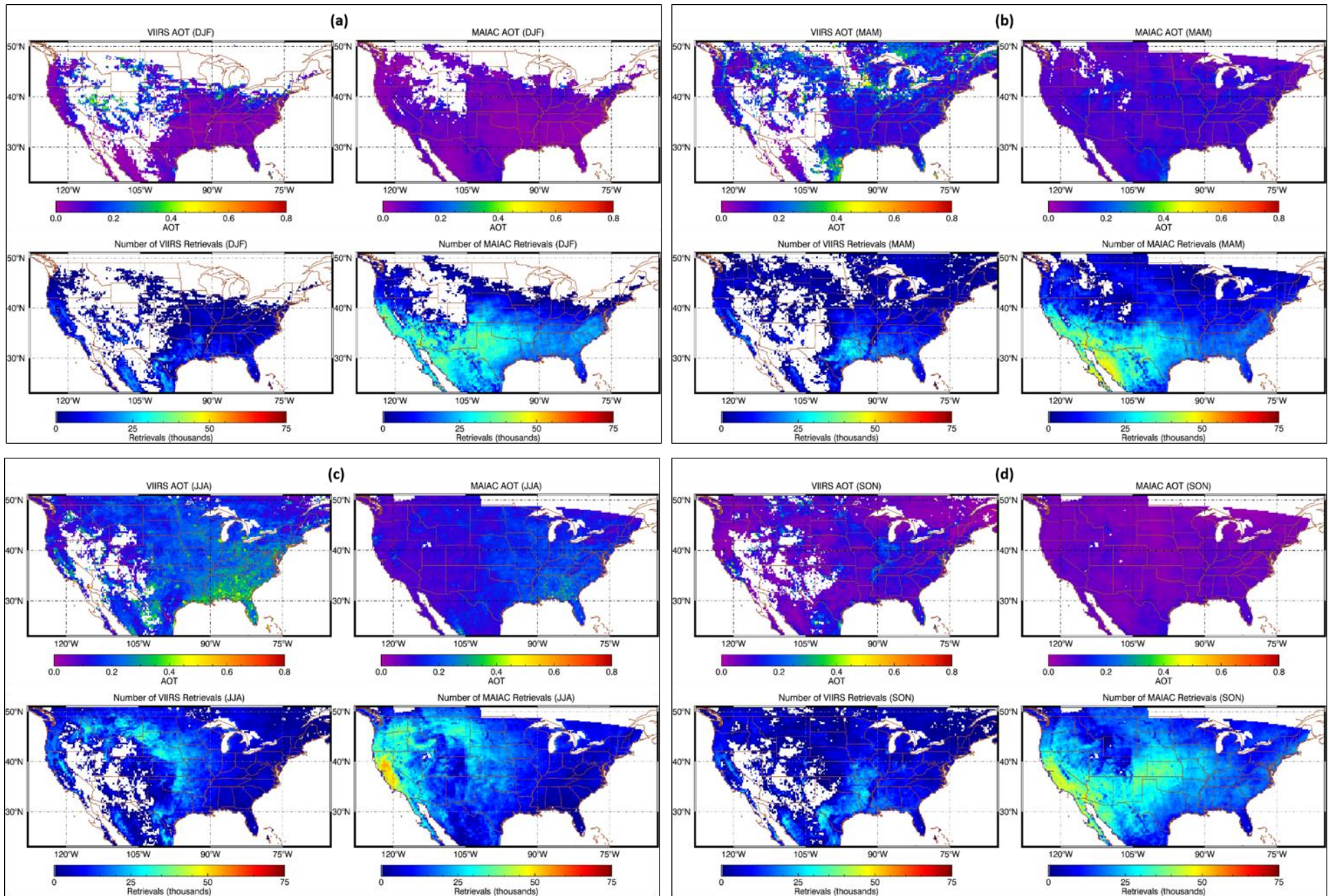
722 **Figures**



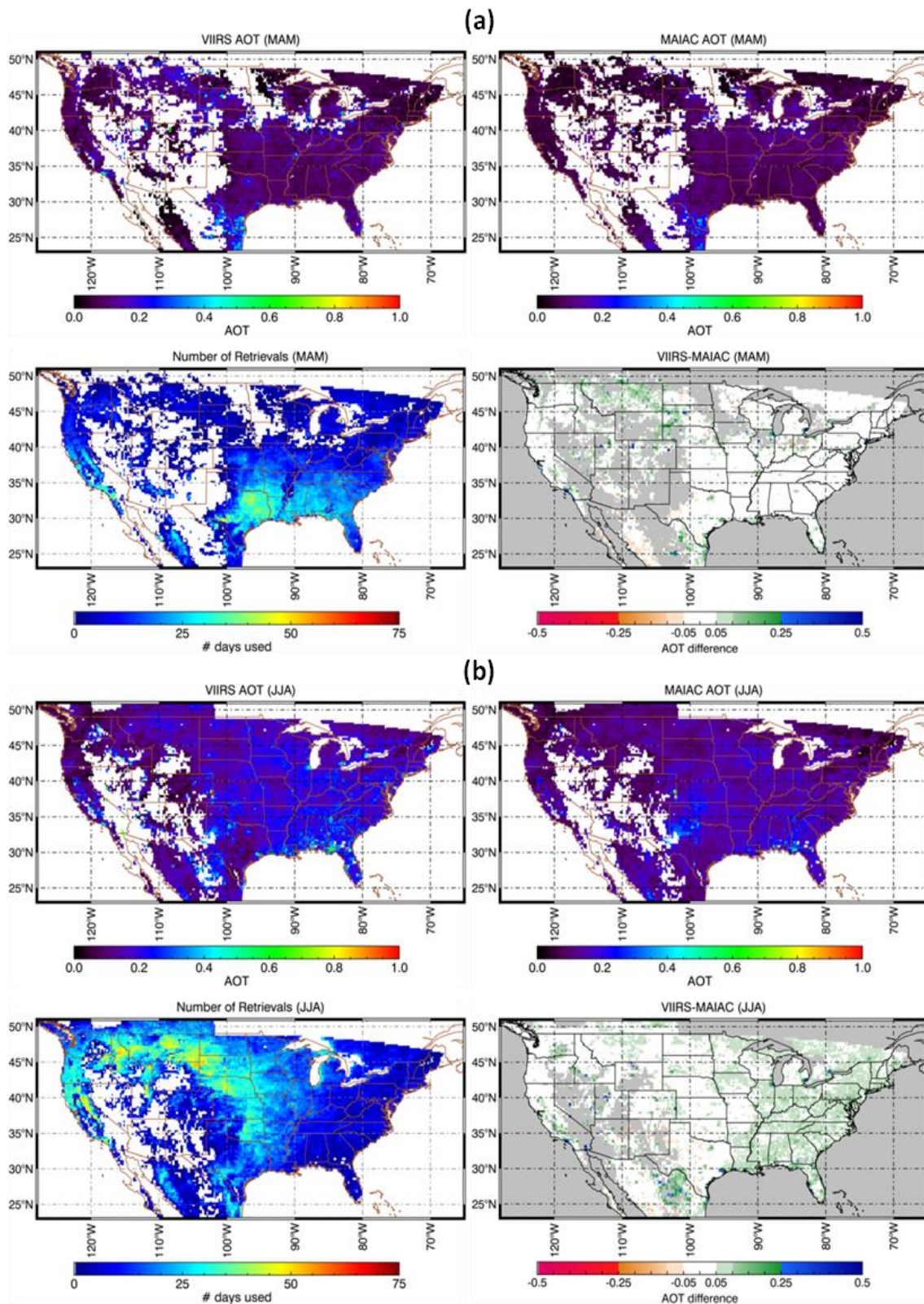
723

724 Figure 1. Map of the domain area used to grid the MAIAC and VIIRS AOT datasets. Domain was
725 chosen based on the extent of MAIAC data currently available over North America. Coordinates of the
726 upper left corner are (51° N, 129° W) and the lower right coordinates are (22° N, 65° W). Map data
727 courtesy of Google Earth Pro (V 7.1.2.2041), Landsat.

728

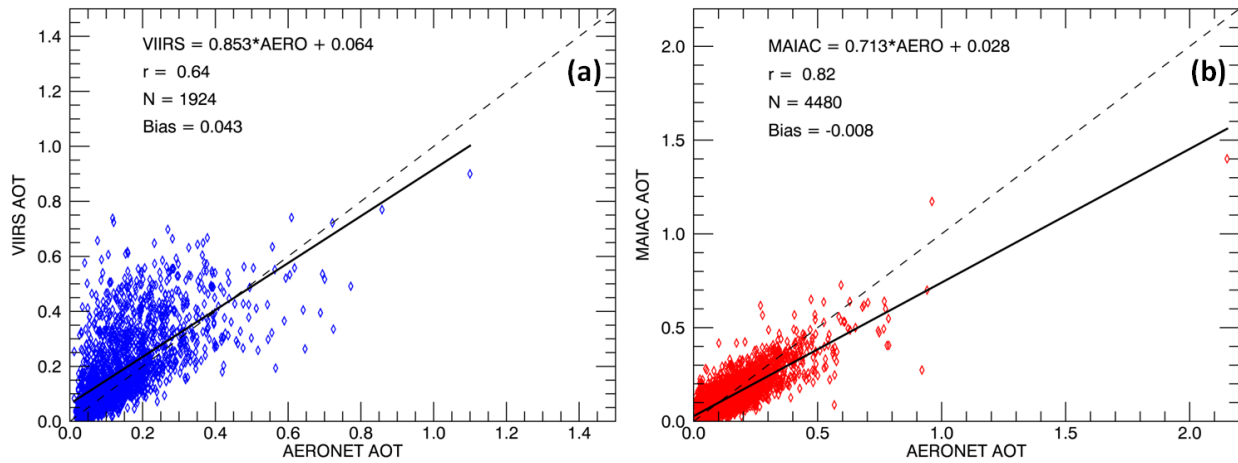


730 Figure 2. Maps of gridded AOT at 550 nm (top) and retrieval count (bottom) from VIIRS and MAIAC for: (a) winter; (b) spring; (c) summer;
731 and (d) fall. Large portions of missing data in MAIAC maps over southern Canada are caused by the geographic extent of available data in
732 this region.



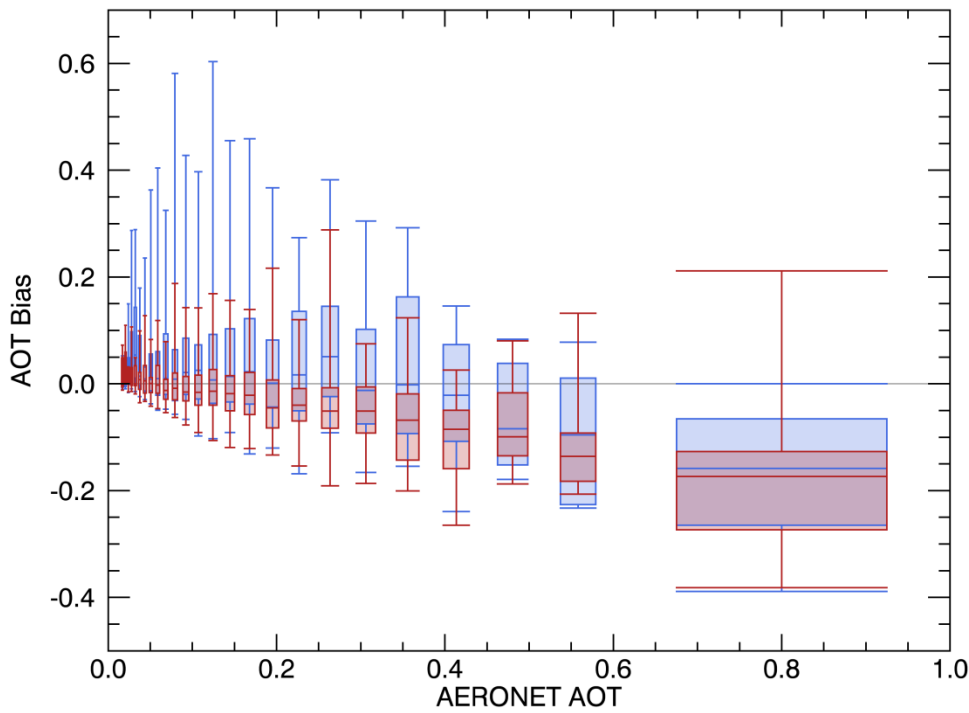
734

735 Figure 3. Set of four-panel plots showing matched VIIRS (upper left) and MAIAC (upper right) AOT
 736 along with number of days with coincident observations (lower left), and AOT difference between the
 737 products (lower right) for the spring (a) and summer (b) seasons.



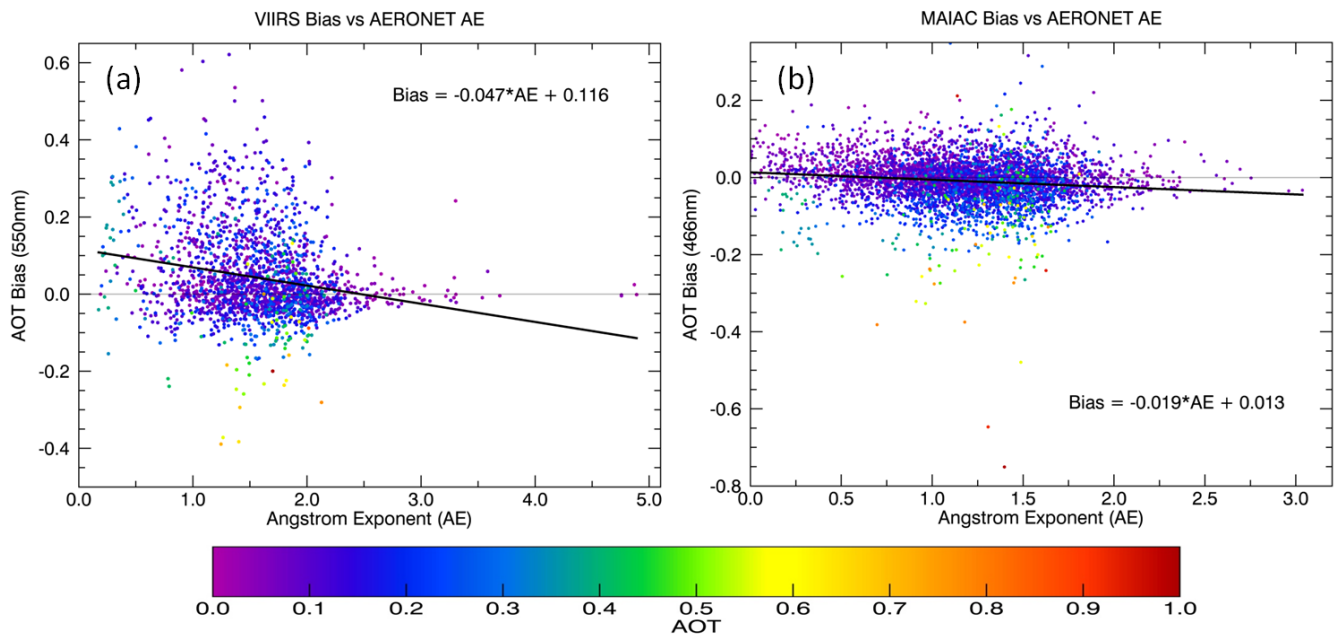
739

740 Figure 4. Scatter plots showing the relationship between AERONET AOT and VIIRS (a) and MAIAC
 741 (b). The dashed line represents the 1:1 line where the two datasets would be in complete agreement,
 742 while the solid lines represent the linear regression model (chi-squared test) provided at the top of each
 743 figure. Relevant relational statistics for correlation, r ; number of observation, N ; and bias are also given.
 744



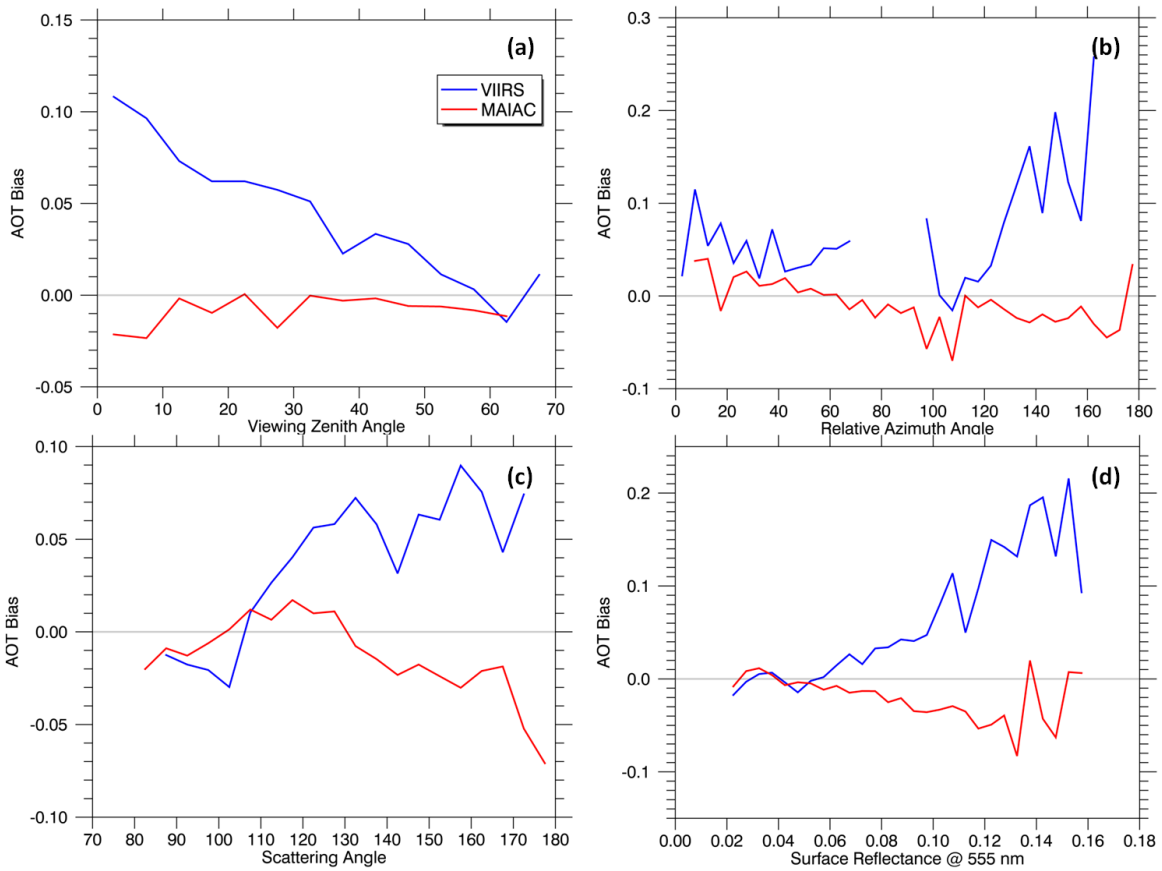
745

746 Figure 5. Box and whisker plot showing the dependence of the VIIRS (blue) and MAIAC (red) bias on
 747 the AOT as measured by AERONET. Any missing data is due to the lack of matchups (< 5) in that
 748 AOT bin.



749

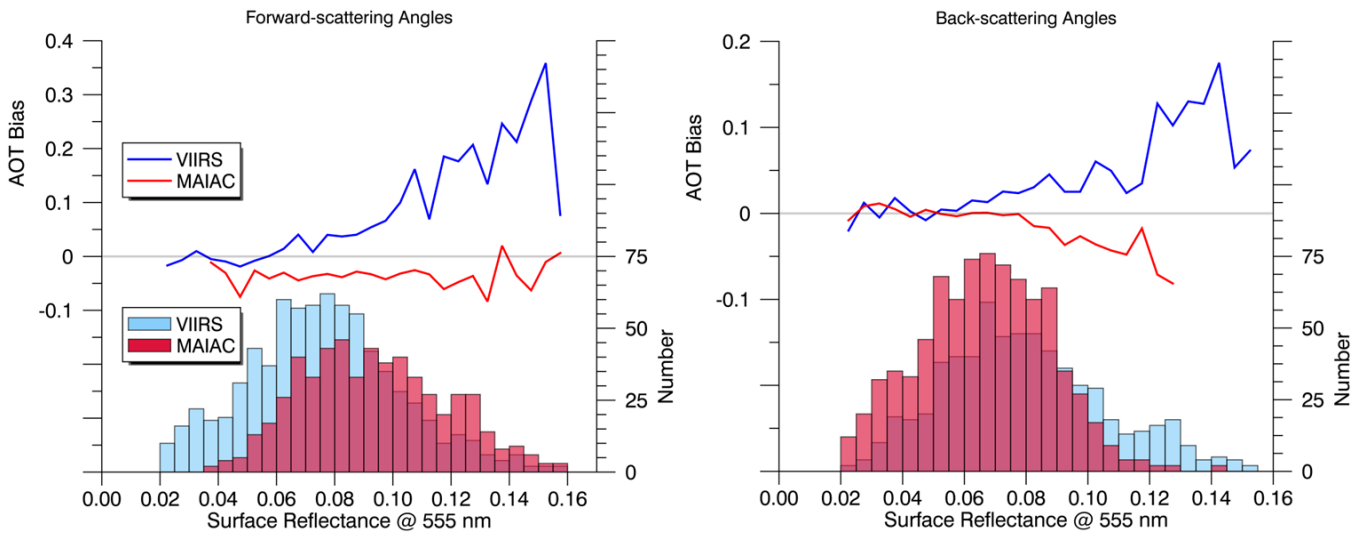
750 Figure 6. AOT errors from the (a) VIIRS, and (b) MAIAC matchups as a function of AERONET
 751 Angstrom Exponent, with regression line drawn in black. Data points are color-coded based on the
 752 AERONET AOT retrieval associated with those matchups.



753

754 Figure 7. Dependence of AOT bias on: (a) viewing zenith angle; (b) relative azimuth angle; (c)
 755 scattering angle; and (d) surface reflectance at 555 nm according to MAIAC. VIIRS data is shown in
 756 blue and MAIAC in red, while the horizontal zero line (gray) is added for reference.

757

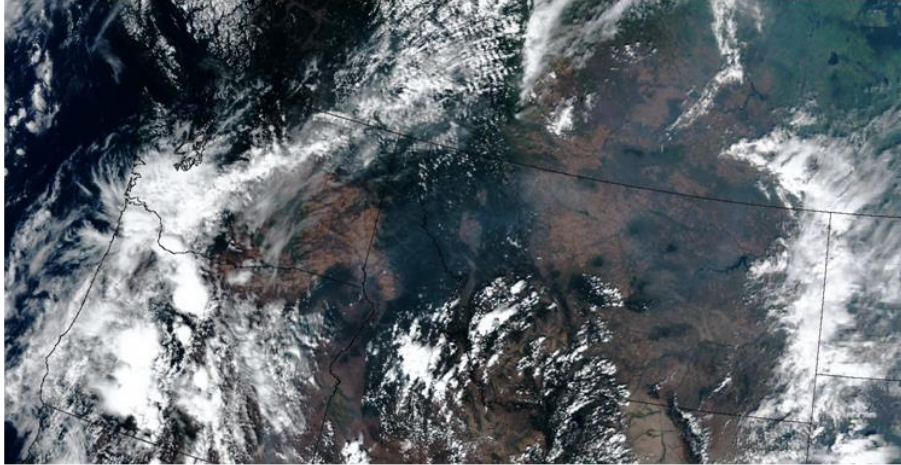


758

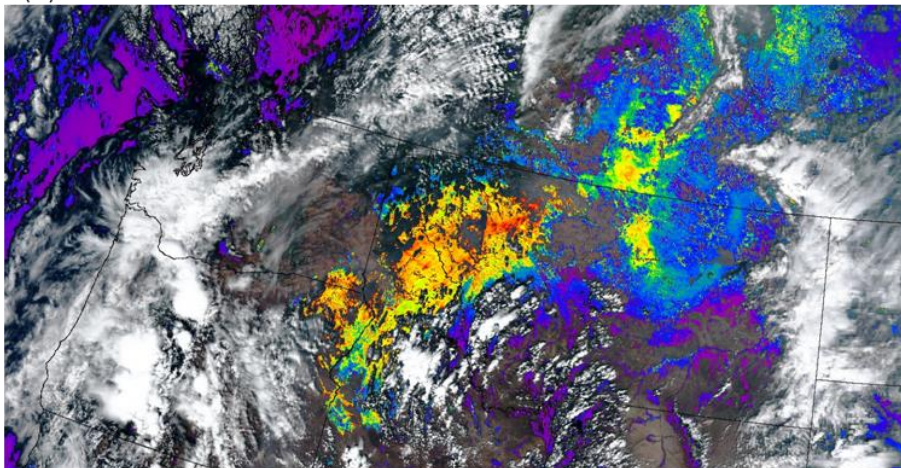
759 Figure 8. Dependencies on surface brightness split into observations taken from the forward-scattering
 760 (left) and back-scattering (right) direction. Bias is on the left-hand vertical axis and represented by the

761 vertical lines, while the number of matchups in each reflectance bin are given by the vertical bars and
762 occupy the right-hand vertical axis.

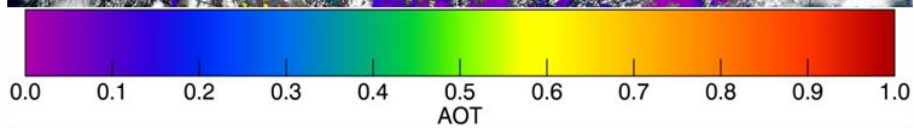
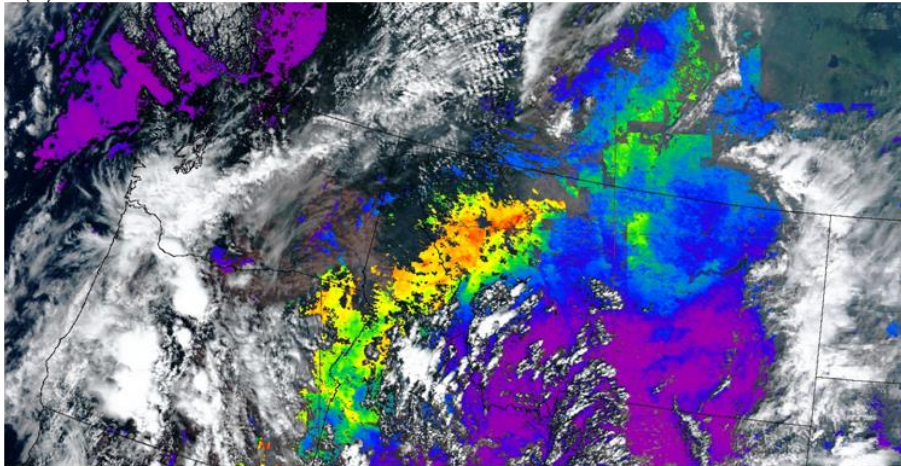
(a) VIIRS True-color Aug. 25th, 2013



(b) VIIRS IP AOT 20:34 - 20:37 UTC



(c) MAIAC AOT 20:20 - 20:25 UTC



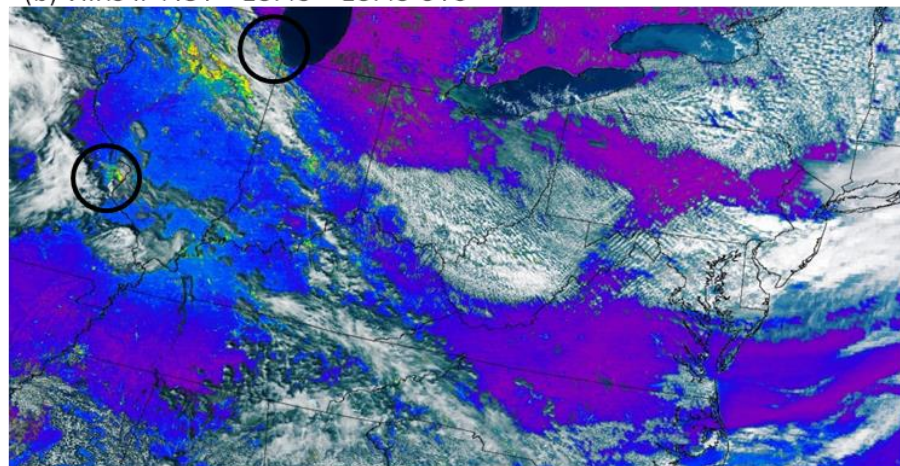
763

764 Figure 9. Example of high aerosol loading on August 25th, 2013 over the western U.S. due to regional
765 fires. (a) True-color image from S-NPP VIIRS; (b) VIIRS high quality IP AOT; (c) MAIAC AOT.

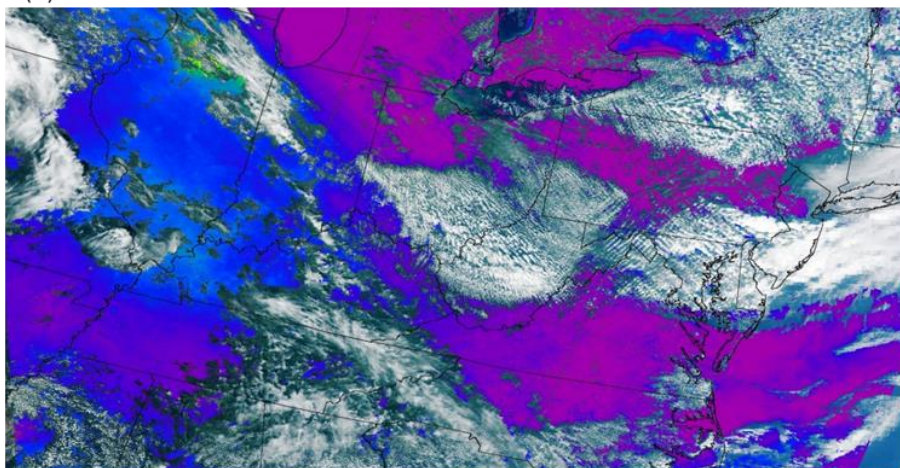
(a) VIIRS True-color Sept. 5th, 2013



(b) VIIRS IP AOT 18:43 – 18:45 UTC



(c) MAIAC AOT 18:20 – 18:25 UTC



0.0 0.1 0.2 0.3 0.4 0.5 0.6 0.7 0.8 0.9 1.0
AOT

766

767 Figure 10. Image of a moderate AOT case from September 5, 2013. (a) True-color image from S-NPP
768 VIIRS; (b) VIIRS high quality IP AOT; (c) MAIAC AOT.